journal

J. Am. Ceram. Soc., 91 [6] 1995–2001 (2008)
DOI: 10.1111/j.1551-2916.2008.02381.x

Mechanical Characterization of Diesel Particulate Filter Substrates

Amit Shyam,*,† Edgar Lara-Curzio,* Thomas R. Watkins,* and Randy J. Parten

Oak Ridge National Laboratory, Materials Science and Technology Division, Oak Ridge, Tennessee 37831

Test procedures for the mechanical evaluation of diesel particulate filter (DPF) substrate materials have been developed and applied for the characterization of porous cordierite under ambient conditions. Specifically the double-torsion test method was employed to characterize fracture toughness and slow crack behavior while resonant ultrasound spectroscopy (RUS) was used to determine the elastic properties of the substrate walls. A dry grinding procedure was developed to fabricate test specimens for these tests. The fracture behavior of porous cordierite was related to the pore structure inside the filter wall. Implications of the test results on the mechanical reliability of DPFs are discussed.

I. Introduction

No standardized techniques exist to evaluate the mechanical properties and fracture behavior of ceramic substrates used for manufacturing diesel particulate filters (DPFs). Most DPFs are honeycomb structures designed to trap particulate matter in the exhaust gas stream of diesel engines. The expected service lifetime of a typical DPF for on-road vehicles is 400 000 miles, and the long-term durability of these devices hinges on their ability to withstand the stresses that are generated during operation, including transients such as filter regeneration. Regeneration refers to the process by which the accumulated particulate matter is removed from a filter. A typical regeneration approach involves heating the filter to combust the particulate matter trapped in the filter pores. Because the particulate matter combustion process is exothermic, a degree of control needs to be exercised during regeneration so that the stresses that result from thermal gradients do not lead to mechanical failure of the filter. Increasingly stringent regulations for NO_x, CO, and particulate matter emissions have prompted research activities to identify and develop materials capable of withstanding the conditions required to meet those regulations.[1] These activities also include efforts to determine the mechanical properties of these materials. The objective of this investigation is to develop procedures for mechanical property evaluation of the walls of a DPF.

Porous cordierite ($Mg_2Al_4Si_5O_{18}$) ceramics, due to their high thermal shock resistance, are leading candidate materials for DPF applications. Pores act as physical traps for particulate matter, and porosity values as high as 50%–70% by volume are typical for cordierite DPF.[2] However, the pores, which are essential for the functional performance of the filter, have a deleterious effect on the mechanical properties of the DPF. This also presents a challenge for the preparation of test specimens for mechanical property evaluation. In this paper, we describe procedures for determining the elastic properties and fracture behavior of porous cordierite used for DPFs. In addition, we describe procedures for the preparation of tests specimens for mechanical property evaluation. The double-torsion testing technique,[3–6] which has been critically reviewed by the authors,[6] was successfully applied to determine the fracture toughness and slow crack growth behavior of porous cordierite under ambient conditions. Recent work has demonstrated that the fracture toughness values calculated by the double-torsion test technique are equivalent to those obtained byASTM-standardized techniques for materials with a flat *R*-curve.[7] Other researchers have proposed techniques for determining the *R*-curve using double-torsion testing geometry.[8] The double-torsion methodology was selected for testing specimens fabricated from the walls of the filter for several reasons, namely (a) the rectangular specimen geometry of double-torsion specimens can be fabricated from the walls of the filter, (b) crack length measurement by optical techniques is difficult in porous cordierite because of the large number of pores, nonreflective nature of the surface, and small crack-opening displacements, and (c) specimen-gripping is difficult for fragile porous cordierite specimens and the double-torsion loading geometry does not require gripping. The parallelism between the surfaces of the double-torsion specimens, however, needs to be high in order to reliably obtain the fracture mechanical properties by double-torsion testing. The high dimensional tolerance of the specimen remains relevant for determining of the elastic properties of the specimen by the nondestructive technique of resonant ultrasound spectroscopy (RUS). The RUS technique[9–11] is well suited for determining of the elastic properties of the plate-shaped substrates fabricated for double-torsion testing. A specimen-preparation procedure was developed that involved holding the porous cordierite double-torsion specimen with a vacuum chuck. The specimen-preparation procedure was critical in obtaining specimens with tight dimensional tolerances, which are required to produce precise fracture toughness and elastic property data for porous cordierite.

There are very few reports of the fracture properties of porous cordierite for filter substrates.[12] Previous studies have reported that this material is susceptible to environmentally-induced cracking,[13] but the slow crack growth exponent of porous cordierite has not been characterized by fracture mechanics testing. The design of reliable and durable cellular DPF structures requires quantification of the mechanical properties of the filter substrates. In addition, the described test procedures can be applied to compare the mechanical properties of filters prepared with different materials and processing conditions.

II. Experimental Procedure

(1) Material and Test Specimen Preparation

The porous cordierite material examined in this study was obtained from a commercially available cylindrical DPF (DuraTrap® CO, Corning Inc., Corning, NY).‡ The DPF was

■ —contributing editor

Manuscript No. 24105. Received December 14, 2007; approved February 1, 2008.
Presented at the 109th Annual Meeting of The American Ceramic Society, Detroit, MI, September 17, 2007 (Energy Materials Symposium).
Research sponsored by the U.S. Department of Energy, Assistant Secretary for Energy Efficiency and Renewable Energy, Office of FreedomCAR and Vehicle Technology Program, as part of the Heavy Vehicle Propulsion Materials Program, under contract DE-AC05-00OR22725 with UT-Battelle LLC. A portion of this research was conducted at the SHaRE User Facility, which is sponsored by the Division of Scientific User Facilities, Office of Basic Energy Sciences, U.S. Department of Energy.
*Member, The American Ceramic Society.
†Author to whom correspondence should be addressed. e-mail: shyama@ornl.gov

‡Certain commercial equipment, instruments, or materials are identified herein in order to specify the experimental procedure adequately. Such identification is not intended to imply recommendation or endorsement by Oak Ridge National Laboratory nor is it intended to imply that the materials or equipment identified are necessarily the best available for the purpose.

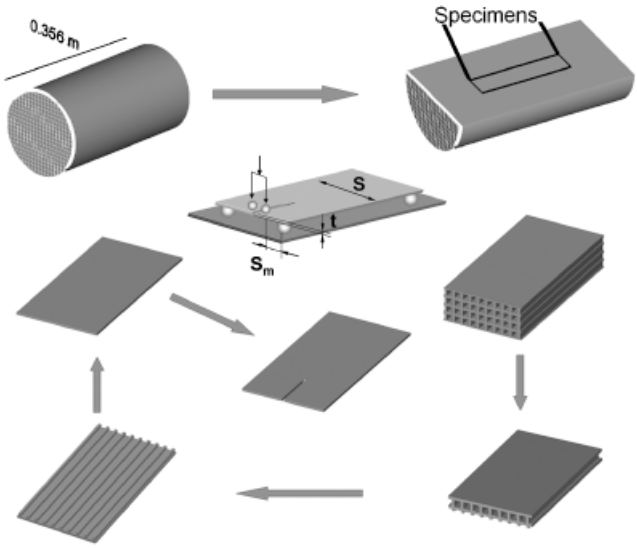

Fig. 1. The sequence of steps followed to prepare plate specimens from the walls of a diesel particulate filter for elastic and fracture property measurements. The ridges on the specimen form as a result of criss-crossing of perpendicular walls and need to be removed in order to prepare flat specimens. The region containing the ridge remains optically visible in the flat specimen because of a change in the orientation of the porosity within this region.

uncoated and had a honeycomb structure with square passage dimensions of about 2.25 mm × 2.25 mm and an initial wall thickness of 0.45 mm. The sequence of steps followed to prepare test specimens for elastic and fracture property testing is schematically illustrated in Fig. 1. The original filter was sliced in half, and rectangular plate-like test specimens were obtained from the central region of the filter, i.e., away from the inlet, outlet, and circumference. A plate with a thickness dimension of one cell (~4.00 mm) was sectioned with a diamond cutoff blade to dimensions of 45.30 mm × 24.50 mm. The single-cell-thickness plate was held by a fixture and ground with a diamond grinding wheel (150 grit, 4000 rpm, 25 μm down feed) to obtain a reference flat surface. The fixture consisted of a precision vise and three gage blocks with pins that fit inside the square passages of the plate. The gage blocks and the blocks holding the plate with a thickness of approximately 4 mm are imaged and shown in Fig. 2. The top surface of the gage block pins defined the initial reference plane.

The plate was subsequently turned upside down and the flat reference surface was placed onto a vacuum fixture designed to hold the test specimen in place while dry grinding in the same conditions described above. The specimen was ground to a thickness such that ridges (from the walls perpendicular to the test specimen, as shown in Figs. 1 and 2) on the specimen were removed completely and a flat specimen thinner than the average wall thickness of the honeycomb structure remained. The fixture obviated the need for glue to bond the test specimen to the grinding fixture. This was beneficial because the glue could be difficult to remove by subsequent cleaning steps and could modify the mechanical properties of the test specimen. By not using glue to hold the specimen during grinding, it was possible to attain a higher degree of specimen parallelism and good control of its thickness. The fixture had two square grooves to evacuate air through the pores in the specimen, and it was found that the final parallelism of the specimen was related to the pressure of the vacuum pump. This behavior is attributed to the fact that a higher pressure bends the compliant test specimen and that some of the ground particles are trapped in the pores of the specimen. The pressure used to hold the specimen was equal to 0.1 MPa (15 psi), which is the smallest pressure that can hold the specimen in place during grinding. Once the flat, ground plates were obtained, several plates were stacked and their sides were

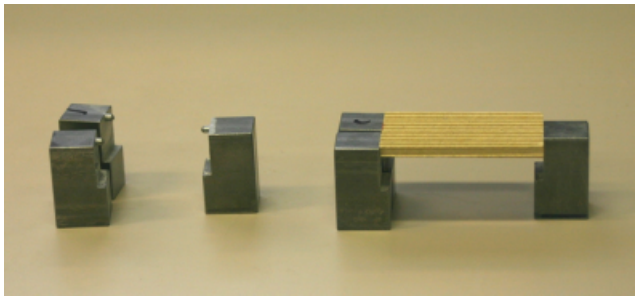

Fig. 2. Image of the gage blocks and the blocks holding the initial plate for grinding. The top surface of the three pins on the gage blocks defined the initial reference plane of the double-torsion specimen.

ground together to obtain plates with dimensions of the double-torsion specimens, i.e., 20.00 mm × 40.00 mm. The mean thickness of all the specimens was 0.375 ± 0.005 mm and the flatness of the specimens was within 8 μm for all the specimens. Previous specimen-preparation techniques involved baking specimens, and in order to be consistent, all the 20 mm × 40 mm plates were baked in a box furnace at 400°C for 4 h. A RUS scan was obtained for every test specimen to determine its elastic properties. To prepare double-torsion test specimens, the ground plates were notched with a thin wafering blade of thickness 0.300 mm on a vacuum fixture, similar to the grinding fixture described earlier. The pressure of the vacuum pump was increased to 0.2 MPa (30 psi) to hold the specimen during notching. The notching fixture had an additional groove to accommodate the wafering blade at the center of the test specimen. The notches were approximately 350 μm wide and 12 mm in length on the compressive face of the double-torsion test specimen and 10.5 mm in length on the tensile face. The tip of the notch was machined to a tapered cross section in order to increase the stress concentration and facilitate precracking at low loads.

(2) Pore and Microstructural Characterization

The microstructure of the filter substrates was characterized with a field emission gun scanning electron microscope (Hitachi S4700/S4800 SEM, Hitachi High Technologies America, Inc., Pleasanton, CA). Two by four cells of the filter were embedded in epoxy and prepared metallographically. To prevent charging, the samples were carbon coated. The porosity of the samples was characterized by standard thresholding and image analysis techniques, following the procedure illustrated in Fig. 3. The dark areas in Fig. 3 correspond to pores and the bright areas correspond to cordierite. The porosity of test specimens subsequently used for double-torsion testing was determined with a pycnometer (Quantachrome Ultrapycnometer 1000, Quantachrome Instruments, Boynton Beach, FL). The bulk density of cordierite was obtained by helium pycnometry. By determining the mass and calculating the volume of the double-torsion specimens, the porosity of the walls was calculated using the following relationship:

$$\text{Porosity}\,(\%) = \frac{\text{Specimen Density}}{\text{Bulk Density}} \times 100 \qquad (1)$$

(3) RUS

RUS was performed for the unnotched double-torsion plates. The experimental set-up consists of a drive piezoelectric transducer and two receiving transducers (Quasar International RI2000, Magnaflux Quasar Systems, Albuquerque, NM). The thin-plate configuration provided a high density of modes in the analyzed frequency range of ~2–30 kHz. The spectra peaks were analyzed using the rectangular parallel-piped model. The elastic modulus, Poisson's ratio, and the root mean square (RMS) error of the fit were calculated by assuming isotropic elasticity and utilizing a weighted nonlinear error minimization software routine (Quasar International RI2000).

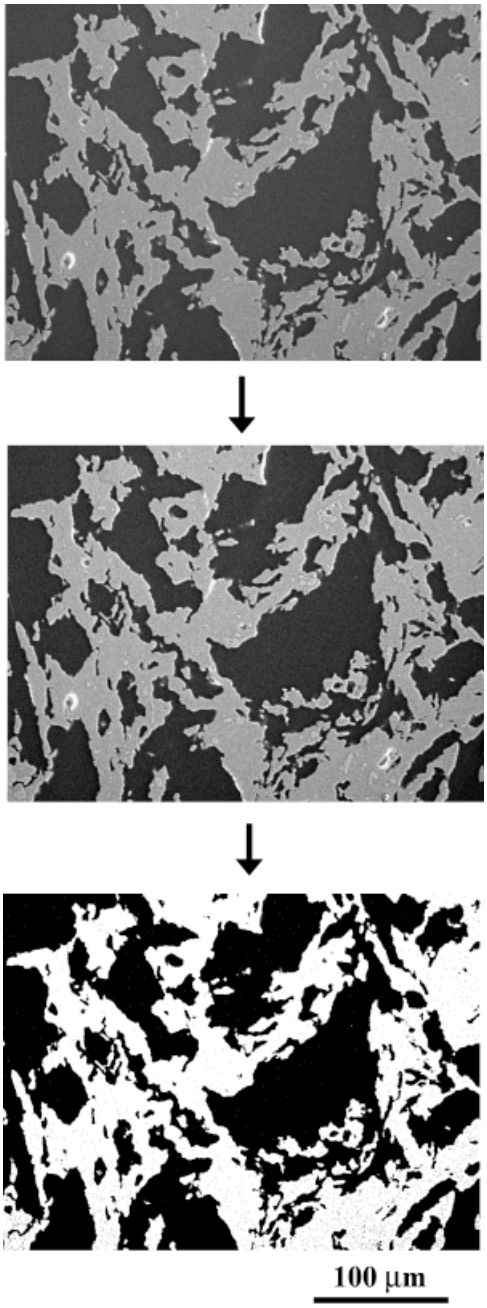

Fig. 3. The procedure for porosity-determination using image analysis techniques. The contrast of the original image is digitally enhanced, and the image is subsequently thresholded and binarized. The percent of black pixels in the binarized image determined the porosity.

(4) Fracture Mechanics Testing

Fracture toughness and slow crack growth experiments were performed under ambient conditions using the double-torsion testing methodology. The partial pressure of water in the laboratory was monitored throughout the testing schedule and it varied between 0.3 and 2.1 kPa (this corresponds to a relative humidity of 13% at 20°C to 65% at 27.2°C). All specimens were precracked at a crosshead displacement rate of 1.0 μm/s in a self-articulating alumina double-torsion fixture[6] and an electromechanical testing machine equipped with computerized data acquisition and control. As shown in Fig. 4, precracking was carried out until there was a noticeable deviation from linearity in the load versus displacement curve. Such deviation from linearity corresponded to an increase in the compliance of the test specimen as a result of initiation of cracking. Typical precraking forces for 0.375-mm-thick specimens were in the range of 0.4–0.6 N (~40–60 gf), illustrating the small forces involved in these

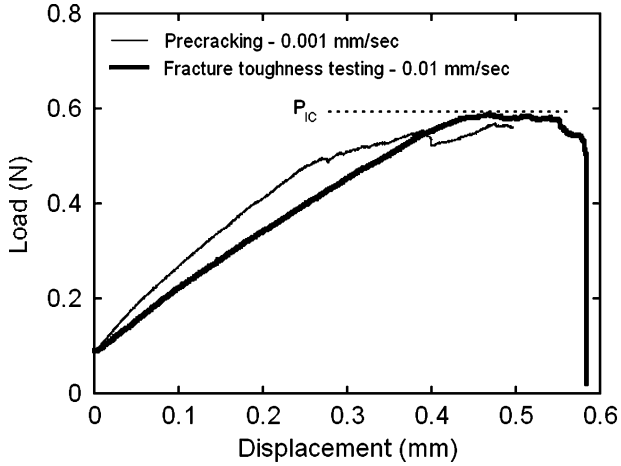

Fig. 4. Load displacement curves for precracking and fracture toughness testing in porous cordierite. The deviation from linearity indicates the formation of a precrack. The 0.1 N dead-load at the start of the test comes from the top portion of the alumina double-torsion fixture.

tests. The tests reported in this paper were carried out using a miniature load cell with a load range of 2.45 N (250 gf) (Model 31—Sensotec®, Model 31: Honeywell Sensotec, Columbus, OH). The precracked specimens were tested at a loading rate of 0.01 mm/s and the fracture toughness was calculated based on the maximum load reached during fracture toughness testing. The loading rate was selected to be sufficiently high while allowing experimental conditions that could be replicated during a controlled slow crack growth test. The test was considered valid only if the crack during fast fracture reached the opposite side with a dimension of 20 mm. If the crack deviated into one of the longer sides of the double-torsion specimen, i.e., if the crack had deviated more than 17° from the notch, the test was considered invalid. It is to be noted in Fig. 4 that the compliance of the precracked specimen is higher than that of the notched specimen and the dead weight of the top portion of the fixture is approximately 0.1 N. Fracture toughness testing was carried out as a function of specimen orientation within the filter.

Slow crack growth testing was performed on the double-torsion test specimens under ambient conditions by the load relaxation method. The specimens were precracked at 1.0 μm/s and then loaded at 0.01 mm/s (same rate as the fracture toughness tests) to 15 gf and allowed to relax for 5 min to account for any potential relaxation in the load train. Subsequently, the specimen was loaded at the same crosshead displacement rate to approximately 90%–95% of the expected fracture load (based on previously determined average fracture toughness values and the geometry of the test specimen), and the crosshead was arrested at that load. Environmentally-assisted crack growth led to a decrease in the load at the fixed crosshead position, and the slow crack growth response of porous cordierite was calculated from the load relaxation curve. The linear crack length versus compliance relationship that is the basis of the double-torsion testing methodology was verified[6] by notching six specimens to notch lengths of 12, 15, 18, 21, 24, and 27 mm and measuring the compliance of those test specimens. Fractography was performed on failed test specimens using a SEM to establish relationships between pore/microstructure and the mechanical properties of the material. The examined fracture surfaces were carbon-coated before SEM examination.

III Results and Discussion

(1) Elastic Property Characterization

RUS[9,10] was performed on the un-notched 20 mm × 40 mm double-torsion plates. Figure 5 is an example spectrum plotted along with the expected resonance frequency of the modes from the calculated isotropic elastic constants. The calculated best fit

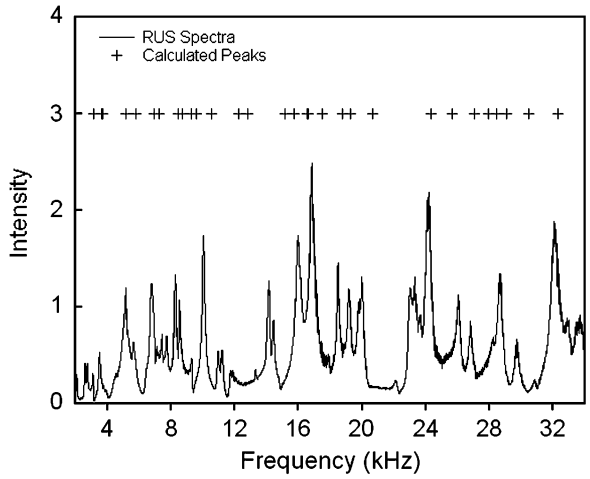

Fig. 5. The experimentally obtained RUS spectra for a plate of porous cordierite under ambient conditions.

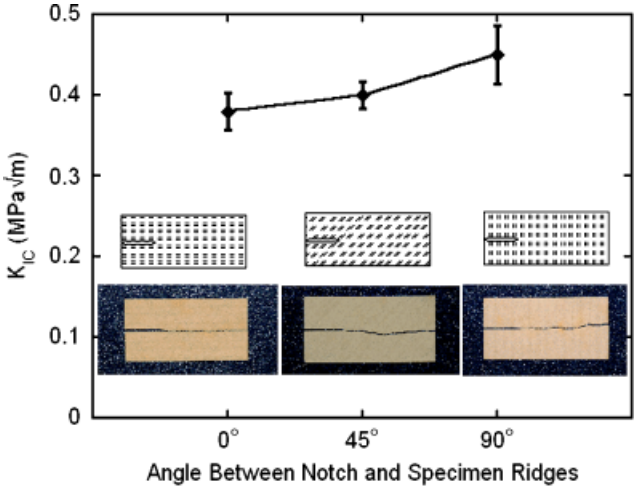

Fig. 6. Effect of specimen orientation on the fracture toughness of porous cordierite. Fracture toughness increased with increasing angle between the crack-propagation direction and specimen ridges. The error bars represent ±SD around the mean values.

for the spectra in Fig. 5 yielded an elastic modulus of 12.16 GPa and a Poisson's ratio of 0.26 with a RMS error of the fit of 2.72%. Similar calculations for 17 other specimens yielded an average elastic modulus of 12.33 ± 0.26 GPa and a Poisson's ratio of 0.24 ± 0.04. The RMS error of the fits for the 17 specimens analyzed was 3.07% ± 0.49%. The RMS error of the fit for the filter substrates is higher than that for bulk materials, where it is typically <1%. The high RMS error of the fit is due to several factors, including splitting of modes because of microcracks in filters, low mass of specimens (0.36–0.38 g) causing inadequate coupling with transducers, and the possibility of elastic anisotropy because of pore morphology. The presence of a different structure in the region that contained the ridges in the specimens is expected to reduce the effective transverse anisotropy from the pores (see Section III*(d)*). The low value of the elastic modulus of porous cordierite demonstrates the lowering of the mechanical performance of the filter substrate because of the presence of porosity.

(2) Fracture Mechanics Testing

The mode I fracture toughness, K_{IC}, for the double-torsion test specimen is independent of crack length (in nearly the middle 40% of the described test specimen geometry) and given by the following expression:

$$K_{IC} = P_{IC} S_m \left(\frac{3(1+\nu)}{S t^4 \psi(\tau)} \right)^{1/2} \tag{2}$$

where P_{IC} is the load at failure, S_m is the moment arm, ν is the Poisson ratio, and S and t are the width and thickness of the double-torsion test specimen, respectively.[4] The dimensions S, t, and S_m are schematically depicted in Fig. 1. In this expression, $\psi(\tau)$ is a finite beam thickness correction factor and is included in order to correct for the interaction of the two torsion bars.[4] $\psi(\tau)$ is a function of the ratio $\tau = 2t/S$, and for $\tau < 1$, a simplified expression with an accuracy better than 0.1 percent is given by

$$\psi = 1 - 0.6302\tau + 1.20\tau \exp(-\pi/\tau) \tag{3}$$

The fracture toughness value of porous cordierite was calculated by substituting the experimentally obtained maximum loads (P_{IC}, as shown in Fig. 4) for the precracked specimens. Equation (2) demonstrates the quantitative significance of high dimensional tolerance of specimens to obtain reliable fracture toughness values with this testing methodology. The control of thickness variation is especially important because fracture toughness is inversely related to the square of the thickness of the test specimen.

The average fracture toughness value from the evaluation of five porous cordierite specimens was found to be 0.38 ± 0.02 MPa√m. These specimens were prepared so that the notches were parallel to the ridges on the test specimen. The effect of the orientation of the notch relative to the orientation of the ridges in the specimen was investigated, and the results are presented in Fig. 6. Five tests were performed in each orientation, and the error bars represent the standard deviation of the values. It can be observed that when the angle between the ridge and the specimen notch increased, the fracture toughness of the filter substrates also increased. The fracture toughness values of specimens in the 45° and 90° orientation are 0.40 ± 0.02 and 0.45 ± 0.04 MPa√m, respectively. The images of tested specimens in the three different orientations along with a schematic demonstrating the orientation of the ridges in the specimens are included in Fig. 6. It is noted that the region containing the ridge can be discerned in the failed specimens shown in Fig. 6 as a result of a change in the orientation of the porosity within this region. The terms "ridges" and "region containing ridges" are used interchangeably for the prepared double-torsion specimens. The increase in fracture toughness values with the angle between the notch and the specimen ridges suggests that the structure in the region that contained the ridges helps increase the resistance of the material to crack propagation. Figure 6 demonstrates the usefulness of the double-torsion testing methodology in measuring fracture property anisotropy within plate-like, rectangular test specimens.

The slow crack growth behavior of porous cordierite was studied for test specimens where the notch is parallel to the ridges under ambient conditions. The load relaxation technique was used to obtain the crack growth velocity ($v = da/dt$) according to the following relationship[3,6]:

$$\nu = \frac{-a_i P_i}{P^2} \frac{dP}{dt} \tag{4}$$

where a_i is the initial crack length, P_i is the initial load or the load value where the relaxation test begins, P is the load value for which the velocity is being calculated, and (dP/dt) represents the slope of the load versus time curve at load P. The initial crack length was back-calculated by inputting the compliance value of the precracked test specimen into the compliance versus crack-length calibration.[6] The stress intensity factor associated with a load value was calculated according to Eq. (2). The continuous load relaxation curve provided a series of ν–K points that represents the slow crack growth behavior of the material, and two ν–K curves are plotted in Fig. 7. The exponents for the

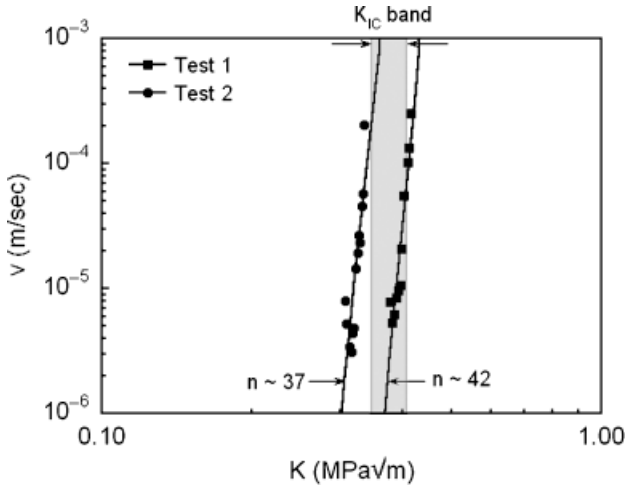

Fig. 7. *v–K* curves for porous cordierite under ambient conditions. The slow crack growth exponents are indicated.

two curves in Fig. 7 were 37 and 43, respectively. These results suggest that the porous cordierite is susceptible to environmentally assisted cracking. The measured slow crack growth exponent values are comparable to a static fatigue exponent of 35 for porous cordierite reported by other researchers.[13] The success rate of performing a fracture mechanics slow crack growth test in porous cordierite was found to be 30%–40%. In other words, some specimens fail before relaxation starts, and in other specimens incomplete relaxation occurs because of a low value of stress intensity factor. The unsuccessful tests are due to the uncertainty from the "K_{IC} band," as indicated in Fig. 7. The center of this band represents the mean of the fracture toughness values, and the width of this band is equal to twice the standard deviation of fracture toughness values. Even though the success rate for performing double-torsion slow crack growth tests may be low, it is a lot easier to obtain the slow crack growth exponent with this test method when compared with the standard ASTM technique, which requires a minimum of 40 specimens to be tested.[14] The possible crack-length dependence on the position of slow crack growth curves obtained by the load relaxation technique has been discussed in detail by the authors.[6]

(3) Porosity Characterization

The porosity of the walls of 2×4 cells of porous cordierite was characterized by image analysis. Figure 8(a) is an image of a metallographically prepared specimen that illustrates the cellular structure of the DPF filter. The circular features in this micrograph are due to shrinkage of the epoxy resin after solidification. Figure 8(b) is a higher magnification image of the wall of the specimen, and image analysis techniques described above were employed to obtain the porosity of this image. The average porosity of 10 images from the region where the double-torsion specimens were fabricated was found to be $49.07\% \pm 2.67\%$ via image analysis. The bulk density of porous cordierite was obtained as 2460 kg/m^3 by helium pycnometry. The porosity of the unnotched double-torsion specimens could alternately be obtained from the bulk density value by utilization of Eq. (1). The average porosity of the double-torsion specimens was found to be $50.00\% \pm 0.33\%$, which corresponds to a specimen density of 1.23 g/cm^3. The standard deviation of the porosity values obtained from image analysis is higher because of the smaller field of view associated with individual images compared with the size of the double-torsion test specimen.

(4) Relationship Between Microstructure and Fracture Properties

The high value of porosity that is necessary for maintaining the functional characteristic of filter substrates lowers their toughness. Model solutions for fracture toughness in a cellular

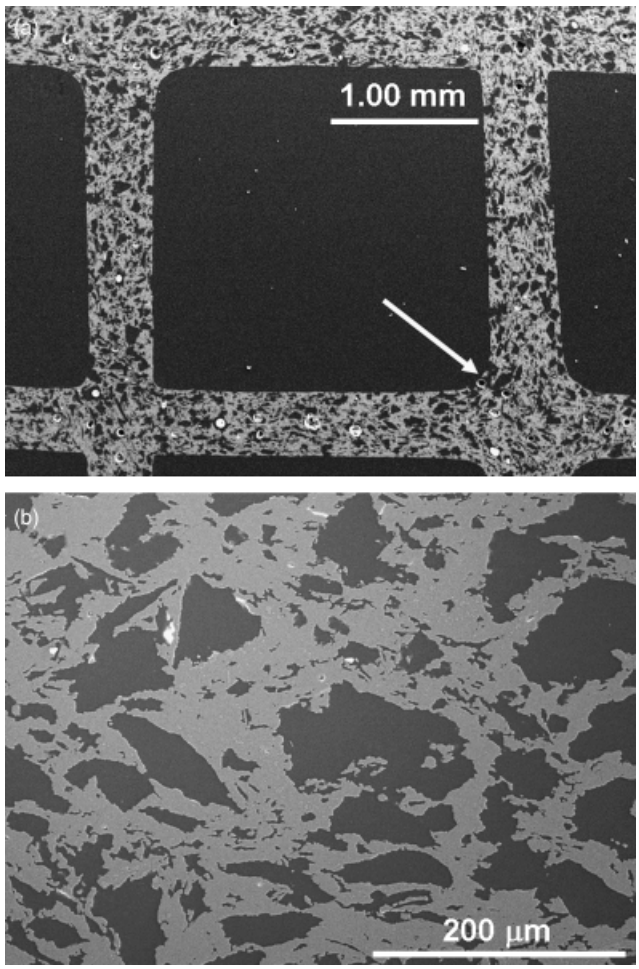

Fig. 8. Scanning electron micrograph of a metallographically prepared specimen showing (a) image of a square passage with the ridge region indicated with an arrow and (b) image of the wall of the specimen showing a slight elongation of the pores parallel to walls of the filter.

structure predict a nonlinear relationship between fracture toughness and porosity.[15] Although the filter substrate has a complex microstructure with more than one phase, extensive porosity, and micro-cracks, the observed variation in the value of fracture toughness of the test specimens due to orientation effects can be attributed primarily to the morphology of the pores. The increase in fracture toughness with increase in angle between the notch and ridges shown in Fig. 6 is due to the change in the local orientation of the porosity of the specimen inside the ridge, which changes the resistance of the material to crack propagation. The arrow in Fig. 8(a) indicates the region that will become a ridge region in a double-torsion test specimen. A slight elongation of the pores parallel to the surface of the walls of the specimen can be observed in Figs. 8(a) and (b). As shown schematically in Fig. 9(a), this minimal elongation of pores makes the ridge area (the area where the perpendicular walls of the filter passages crisscross) a region of increased stress concentration and hence preferential crack propagation in the orientation where the notch and the crack-propagation direction are parallel to the ridge. The stress concentration due to an ellipse is higher if the stress is applied perpendicular to the major axis of the ellipse.[16] The elongation of the pore shape in Fig. 9 has been exaggerated for the purpose of illustration. These same ridges, however, provide a toughening mechanism in other orientations such as Fig. 9(b), with the material resistance to crack propagation increasing with the angle between the ridge and the starter notch.

The intimate relationship between the porosity and fracture characteristic of filter substrate can be observed in Fig. 10. Figure 10(a) is a SEM image of a precrack that has initiated

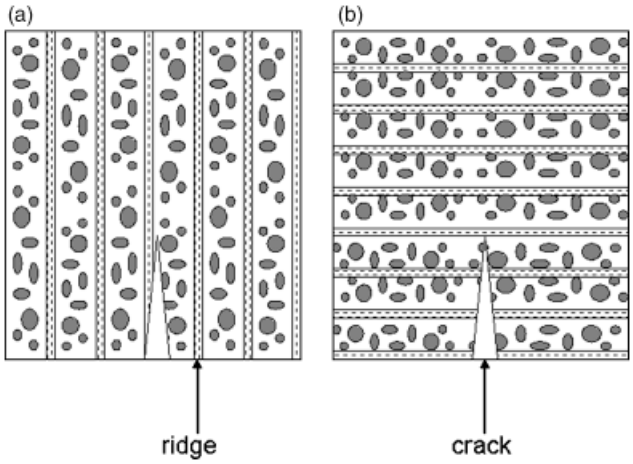

Fig. 9. Schematic figures showing the interaction of a crack with the ridges in orientations where (a) the crack propagation direction is parallel to the ridge and (b) crack propagation direction is perpendicular to the ridge.

from the notch of a double-torsion specimen. As expected, the crack extends by joining larger pores in its path, thereby minimizing the creation of new surfaces as per the Griffith criterion. Figure 10(b) is a SEM image of the fracture surface of the tested double-torsion specimen where the presence of a distribution of pore sizes can be observed. In Fig. 10(b), there are several flat and featureless areas on the fracture surface where the ligaments of the cellular structure have broken as a result of crack propagation.

As shown previously, changing characteristics such as orientation in the specimens can lead to a change in the average fracture toughness by about 20% (0.38–0.45 MPa$\sqrt{}$m in Fig. 6). It is to be noted that any comparison with values in the literature should account for the fact that the porosity of cordierite substrates for DPF applications can vary widely. For example, the values obtained in this study are comparable to a stress intensity value of 0.56 MPa$\sqrt{}$m (where unstable fracture occurs on the *R*-curve) for porous cordierite, with 43% porosity.[12] Several studies on the fracture toughness of dense cordierite indicate a room-temperature fracture toughness value in the range of 2–3 MPa$\sqrt{}$m.[17,18]

The susceptibility of cordierite to slow crack growth is attributed to the presence of an amorphous phase at the grain boundaries.[19] Kaneko *et al.*[19] have reported the presence of amorphous phases at the grain boundary of porous cordierite that is responsible for the delayed failure of this material in environments containing water vapor. Cordierite is a silicate-based ceramic and the low value of slow crack growth exponent reported in this study and in the literature[13] is due to the ability of water molecules to attack the grain boundary glassy phase, causing environmentally-assisted failure.

(5) Implications for Mechanical Reliability of Filters

Diesel particulate filtration devices are designed to operate at elevated temperatures. Although the thermal expansion and thermal shock resistance[20–23] of cordierite for filter substrates have been reported earlier, not much is known about the fracture behavior of these materials at elevated temperature. The methodologies reported in this manuscript have been applied to investigate the fracture behavior of the DPF substrates at elevated temperature, and the results will be reported in the future. The results reported in this paper, such as the orientation effects on fracture toughness, are nevertheless relevant for all operating temperatures. For example, the circumferential nature of ring cracks that form during regeneration means that orientation effects on fracture are important in determining the reliability of DPFs. As shown in Fig. 7, the filter substrate is susceptible to slow crack growth under ambient conditions. The slow crack growth exponent is a critical input for any life prediction model for this device and needs to be characterized under relevant operating conditions. In addition to the variables considered in the present investigation, it is to be noted that the filter is a

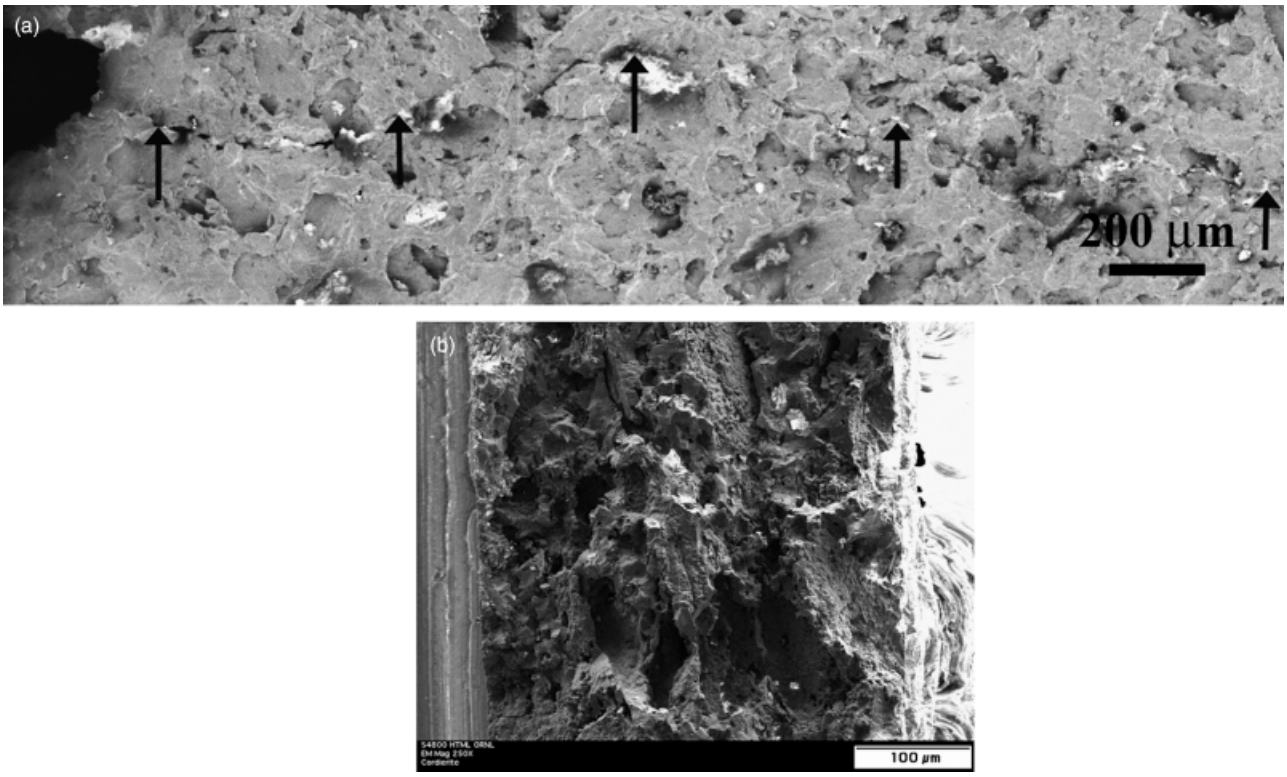

Fig. 10. (a) Scanning electron micrograph from the tensile side of a double-torsion specimen showing the precrack initiated from the tip of the machined notch on the far left of the figure. The direction of crack growth is from left to right. (b) Image of the fracture surface showing pores and flat areas of transgranular failure. The direction of crack growth is from bottom to top.

honeycomb structure. Earlier work suggests that the fracture toughness of honeycomb structures may be related to cell size,[24] and this is an avenue for future efforts to refine the lifetime prediction model of ceramic particulate filters.

IV. Conclusion

Test procedures were developed for the elastic and fracture property characterization of DPF substrates. The procedures were implemented on the walls of a porous cordierite ceramic particulate filter. Fracture toughness of porous cordierite was found to be a function of the orientation within the test specimen, and the values ranged from 0.38 to 0.45 MPa$\sqrt{m}$. Porous cordierite was found to be susceptible to slow crack growth under ambient conditions. The elastic modulus of porous cordierite determined by RUS was found to be 12.33 GPa. The elastic and fracture behavior of the analyzed material was intimately related to the size and morphology of the pores within the walls of the filter. The specimen-preparation procedure that was developed for this investigation was a key factor in enabling mechanical characterization of DPF substrates.

Acknowledgments

The authors are grateful for valuable discussions with their colleagues Tom Yonushonis, Randy Stafford, and Cheryl Klepser of Cummins, and Craig Litwiler, Sujanto Widjaja, Jim Webb, and Gagik Parsamian of Corning. The authors thank Andrew Wereszczak (ORNL) and Hong Wang (ORNL) for reviewing the manuscript.

References

[1]United States Environmental Protection Agency. "Questions and Answers on Using a Diesel Particulate Matter Filter in Heavy-Duty Trucks and Buses"; United States Environmental Protection Agency, Office of Transportation and Air Quality EPA420-F-03-017, June 2003.

[2]I. Melscoet-Chauvel, C. Remy, and T. Tao, "High Porosity Cordierite Filter Development for NO_x/PM Reduction," *Ceram. Eng. Sci. Proc.*, **26** [8] 11–9 (2005).

[3]D. P. Williams and A. G. Evans, "A Simple Method for Studying Slow Crack Growth," *J. Test. Eval.*, **1** [4] 264–70 (1973).

[4]E. R. Fuller Jr., "An Evaluation of Double-Torsion Testing–Analysis"; pp. 3–18 in *Fracture Mechanics Applied to Brittle Materials - ASTM STP 678*, Edited by S. W. Freiman. American Society for Testing and Materials, Philadelphia, PA, 1979.

[5]B. J. Pletka, E. R. Fuller Jr., and B. G. Koepke, "An Evaluation of Double-Torsion Testing-Experimental"; pp. 19–37 in *Fracture Mechanics Applied to Brittle Materials - ASTM STP 678*, Edited by S. W. Freiman. American Society for Testing and Materials, Philadelphia, PA, 1979.

[6]A. Shyam and E. Lara-Curzio, "The Double-Torsion Testing Technique for the Determination of Fracture Toughness and Slow Crack Growth Behavior of Materials: A Review," *J. Mater. Sci.*, **41** [13] 4093–104 (2006).

[7]J. A. Salem, M. Radovic, E. Lara-Curzio, and G. Nelson, "Fracture Toughness of Thin Plates by the Double-Torsion Test Method," *Ceram. Eng. Sci. Proc.*, **27** [2] 63–73 (2007).

[8]M. E. Ebrahimi, J. Chevalier, and G. Fantozzi, "*R*-Curve Evaluation and Bridging Stress Determination in Alumina by Compliance Analysis," *J. Eur. Ceram. Soc.*, **23** [6] 943–9 (2003).

[9]R. G. Leisure and F. A. Willis, "Resonant Ultrasound Spectroscopy," *J. Phys.: Condens. Mater.*, **9** [28] 6001–29 (1997).

[10]A. Migliori, J. L. Sarrao, W. M. Visscher, T. M. Bell, M. Lei, Z. Fisk, and R. G. Leisure, "Resonant Ultrasound Spectroscopic Techniques for Measurement of the Elastic Moduli of Solids," *Phys. B*, **183** [1–2] 1–24 (1993).

[11]M. Radovic, E. Lara-Curzio, and L. Riester, "Comparison of Different Experimental Techniques for Determination of Elastic Properties of Solids," *Mater. Sci. Eng. A*, **368** [1–2] 56–70 (2004).

[12]Y. Sakaida and K Tanaka, "Evaluation of Fracture Toughness of Porous Ceramics," *JSME Int. J. Ser. A*, **46** [1] 30–9 (2003).

[13]T. Kuki, Y. Miyairi, Y. Kasai, M. Miyazaki, and S. Miwa, "Study on Reliability of Wall-Flow Type Diesel Particulate Filter"; SAE paper no. 2004-01-0959, 2004.

[14]ASTM Standard C1368, 2006, "Standard Test Method for Determination of Slow Crack Growth Parameters of Advanced Ceramics by Constant Stress-Rate Flexural Testing at Ambient Temperature," ASTM International, West Conshohocken, PA, www.astm.org.

[15]S. K. Maiti, M. F. Ashby, and L. J. Gibson, "Fracture Toughness of Brittle Cellular Solids," *Scr. Metall.*, **18** [3] 213–8 (1984).

[16]C. E. Inglis, "Stresses in a Plate Due to the Presence of Cracks and Sharp Corners," *Trans. Inst. Naval Architects*, **55**, 219–41 (1913).

[17]G. A. Gogotsi, V. P. Zavada, and F. Y. Kharitonov, "Strength and Crack Resistance of Ceramics. Report No. 1. Cordierite," *Strength Mater.*, **16** [12] 1651–5 (1984).

[18]H. Suzuki, K. Ota, and H. Saito, "Mechanical Properties of Alkoxy-Derived Cordierite Ceramics," *J. Mater. Sci.*, **23** [5] 1534–8 (1988).

[19]K. Kaneko, N. Honbe, M. Matsumoto, Y. Yasutomi, T. Saitoh, and Y. Takigawa, "Triple-Layered, Thick Glassy Grain Boundaries in Porous Cordierite Ceramics," *Acta Mater.*, **50** [3] 597–604 (2002).

[20]D. L. Evans, G. R. Fischer, J. E. Geiger, and F. W. Martin, "Thermal Expansions and Chemical Modifications of Cordierite," *J. Am. Ceram. Soc.*, **63** [11–12] 629–34 (1980).

[21]S. Kitaoka, Y. Matsumisha, C. Chen, and H. Awaji, "Thermal Cyclic Fatigue Behavior of Porous Ceramics for Gas Cleaning," *J. Am. Ceram. Soc.*, **87** [5] 906–13 (2004).

[22]I. M. Lachman, R. D. Bagley, and R. M. Lewis, "Thermal Expansion of Extruded Cordierite Ceramics," *Ceram. Bull.*, **60** [2] 202–5 (1981).

[23]E. Lucchini and S. Maschio, "Thermal Shock Resistance of Cordierite Filter for Diesel Engines," *Mater. Sci. Tech.*, **11** [6] 605–10 (1995).

[24]J. S. Huang and L. J. Gibson, "Fracture Toughness of Brittle Honeycombs," *Acta Metall. Mater.*, **39** [7] 1617–26 (1991). □